

Accepted by *Geophysical Research Letters*, 1995.

Formation, Propagation, and Decay of Coherent Pulses of Solar Cosmic Rays

D. Ruffolo and T. Khumlumlert
Chulalongkorn University, Thailand

Abstract

We have performed numerical simulations of the interplanetary transport of solar cosmic rays. The particles form a coherent pulse within ~ 0.01 AU after their injection. The gradual decrease of a pulse's speed and anisotropy can be understood in terms of an equilibrium between pitch-angle scattering and focusing. The results should be useful for estimating times of particle injection.

Introduction

Much of the current research on solar cosmic rays aims to determine the time distribution of their emission during solar flares. The major obstacle is that no spacecraft has approached closer than ≈ 0.3 AU from the Sun, so interplanetary scattering has greatly broadened the observed temporal distributions. This problem is least severe when the detector is magnetically reasonably well-connected to the flare. If strong anisotropies are observed, they also aid the determination of the scattering mean free path and the injection profile (Kallenrode, Wibberenz, and Hucke 1992).

The key phenomenon underlying the strong anisotropy observed for many well-connected events is that charged particles of a given energy tend to travel together as a highly anisotropic "coherent pulse," which can survive long enough to be observed near the Earth. Figure 1 shows stages in the formation of such a pulse very close to the Sun. This phenomenon was first systematically described by Earl (1974, 1976a, b) who used analytic approximations to describe their formation and decay. However, that description was limited by the assumption of a constant focusing length, implying an exponentially decaying magnetic field strength. Here we re-examine the evolution of coherent pulses of solar cosmic rays using numerical simulations for a more realistic Archimedean spiral field (Parker 1958).

Theory and Numerical Method

For ions of $\gtrsim 20$ MeV/n or electrons of $\gtrsim 10$ keV, the transport along the interplanetary magnetic field is well described by the following equation (using the notation of Ng & Wong 1979):

$$\begin{aligned} \frac{\partial F(t, \mu, z)}{\partial t} = & -\mu v \frac{\partial F(t, \mu, z)}{\partial z} \\ & - \frac{v}{2L(z)} \frac{\partial}{\partial \mu} [(1 - \mu^2) F(t, \mu, z)] \\ & + \frac{\partial}{\partial \mu} \left[\frac{\varphi(\mu)}{2} \frac{\partial F(t, \mu, z)}{\partial \mu} \right], \end{aligned} \quad (1)$$

where z is the arclength along the magnetic field, μ is the cosine of the pitch angle (v_z/v), F is the distribution function, defined as the number of particles per z per μ in a given magnetic flux tube, L is the focusing length, $B/(dB/dz)$, and φ is the coefficient of pitch-angle scattering. The first term on the right hand side of eq. (1) expresses the streaming of particles along the magnetic field. The second term is due to pitch-angle scattering from irregularities in the magnetic field, and the final term is due to adiabatic focusing (Roelof 1969).

We derive the focusing length, $L(z)$, from an Archimedean spiral field that makes a 45° angle with the radial direction at a radius of 1 AU, corresponding to a solar wind speed of ≈ 400 km/s. The pitch-angle scattering coefficient, $\varphi(\mu)$, is parameterized as

$$\varphi(\mu) = A|\mu|^{q-1}(1 - \mu^2). \quad (2)$$

following Jokipii (1971). We express our results in terms of the scattering mean free path, λ , which is given by

$$\lambda = \frac{3}{(2 - q)(4 - q)} \frac{v}{A}. \quad (3)$$

Note that for a constant value of λ , eq. (1) involves only the distance traveled, $s = vt$, and not v or t alone. We will therefore show results in terms of s instead of time.

The numerical method used to solve eq. (1) was essentially the finite difference method of Ruffolo (1991), with some minor improvements. That study described tests of the code and successful fits to the observed intensity and pitch-angle distribution as a function of time for neutron-decay protons. More recently, this and two completely different numerical methods were shown to give very similar results (Earl et al. 1995).

Results

Numerical simulations were performed for an initial condition corresponding to an instantaneous injection of particles near the Sun at $t = 0$. For most of the simulations, we took the initial pitch-angle distribution to be concentrated at the highest μ -grid value, and used an absorbing boundary condition at $z = 0$, i.e., $F(t > 0, \mu > 0, z = 0)$ was set to zero. (The injection site and inner boundary, $z = 0$, was set to $r = 0.01 \text{ AU} \approx 2R_{\odot}$ to avoid a divergence in the focusing term.) The outer boundary was set to the maximum value of $s = vt$. Finally, the grid spacings were $\Delta s = 0.02 \text{ AU}$, $\Delta\mu = 0.08$, and $\Delta z = \Delta\mu\Delta s = 0.0016 \text{ AU}$ except where noted.

To examine the propagation of coherent pulses, we plot the average distance along the magnetic field of the particle distribution, $\langle z \rangle$, as a function of $s = vt$ for selected values of λ and q (Figure 2). The dashed line, $\langle z \rangle = s$, shows where the particles would be if they all traveled directly along the magnetic field, with $\mu = 1$ and $v_z = v$. As expected, the progress along the magnetic field is fastest for the longest mean free path, corresponding to the weakest scattering.

The rate of change of $\langle z \rangle$ with respect to s is

$$\frac{d\langle z \rangle}{ds} = \langle \mu \rangle = \frac{\delta}{3}, \quad (4)$$

where δ is the anisotropy averaged over the particle distribution, so $\langle \mu \rangle$ is proportional to the pulse's propagation speed and anisotropy. Figure 3a shows the evolution of $\langle \mu \rangle$ as a function of the average position, $\langle z \rangle$. The most noticeable trend is that $\langle \mu \rangle$ monotonically decreases with position in all cases, as the pulse moves to regions where the focusing is weaker. This slowing in turn causes the curvature of the lines in Figure 2 away from the line of maximum speed.

Another noticeable feature in Figure 3a is the convergence of curves for different q toward a universal curve for smaller $\langle \mu \rangle$ values. This convergence occurs later for higher values of λ and always appears at similar values of $\langle \mu \rangle$, indicating that the convergence coincides with the decay of the coherent pulse toward a diffusive distribution. This can be verified by examining $\sigma_z = \sqrt{\langle (z - \langle z \rangle)^2 \rangle}$ (Figure 3b). We note that the position at which $\sigma_z = \langle z \rangle / 4$ (long-dashed line) for each λ corresponds roughly to the position of convergence, and to a value of $\langle \mu \rangle \approx 1/3$. We will therefore refer to $\langle \mu \rangle \gtrsim 1/3$ as the coherent pulse régime and to $\langle \mu \rangle \lesssim 1/3$ as the diffusive régime.

The behavior of $\langle \mu \rangle$ vs. $\langle z \rangle$ can be interpreted in

terms of an equilibrium between the scattering and focusing terms in eq. (1) with the streaming term “turned off.” [The scattering/focusing eigenfunctions defined by Earl (1976a) used a different form of eq. (1), and thus have a different physical interpretation.] Figure 4 shows simulation results for the equilibrium average of the pitch-angle cosine, $\langle \mu \rangle_{eq}$, and the equilibration distance, s_{eq} , which is the distance traveled over which equilibrium is achieved, or v times the longest relaxation time. The results for $\langle \mu \rangle_{eq}$ are in good agreement with the analytic expression

$$\langle \mu \rangle_{eq} = \frac{\int_{-1}^1 \mu F_{eq} d\mu}{\int_{-1}^1 F_{eq} d\mu} = \frac{\int_{-1}^1 \mu \exp\left(\frac{v}{AL} \frac{\mu|\mu|^{1-q}}{2-q}\right) d\mu}{\int_{-1}^1 \exp\left(\frac{v}{AL} \frac{\mu|\mu|^{1-q}}{2-q}\right) d\mu} \quad (5)$$

(fortunately, for the q values chosen here, these integrals can be solved in terms of simple functions). For large z (i.e., $L \gg \lambda$, or the weak focusing limit), s_{eq} approaches a q -dependent value (equal to or slightly larger than λ) which agrees with the $L = \infty$ value of Bieber (1978).

For very small values of z , where there is very strong focusing, s_{eq} is also small, and the distribution achieves pitch-angle equilibrium very quickly. At the same time, $\langle \mu \rangle_{eq} \approx 1$, so the distribution “relaxes” rapidly (within $\sim 0.01 \text{ AU}$) to form a coherent pulse with nearly maximal anisotropy and highly collimated motion along the magnetic field (Figures 1 and 5; a finer grid spacing was used for these simulations). Note that the spiky features in Figure 1, before pitch-angle equilibrium is reached, are due to the low scattering coefficient, $\varphi(\mu)$, near $\mu = 1$. Initial injections that were isotropic or highly focused yielded essentially the same distribution beyond $z = 0.03 \text{ AU}$, with the former lagging by only 0.004 AU . A reflecting boundary condition gave virtually identical results.

Farther from the Sun, we see that $\langle \mu \rangle_{eq}$ rapidly declines with z (Figure 4). Since the equilibration distance rapidly increases, the pitch-angle equilibrium is not maintained and $\langle \mu \rangle$ declines less rapidly. For a narrow pulse, the deviation from pitch-angle equilibrium evolves according to

$$\frac{d(\langle \mu \rangle - \langle \mu \rangle_{eq})}{ds} = -\frac{\langle \mu \rangle - \langle \mu \rangle_{eq}}{s_{eq}} - \langle \mu \rangle \frac{d\langle \mu \rangle_{eq}}{dz}. \quad (6)$$

However, this equation gives a steady-state deviation which is insufficient to account for the difference between $\langle \mu \rangle$ and $\langle \mu \rangle_{eq}$ in the diffusive régime. The remaining deviation can be explained by considering

the width of the distribution. During the diffusive phase, the average of $\langle \mu \rangle_{eq}$ over the distribution can deviate significantly from the value at $\langle z \rangle$. Thus we see that the convergence of $\langle \mu \rangle$ as a function of $\langle z \rangle$ for different q 's in the diffusive phase is due to 1) the convergence of $\langle \mu \rangle_{eq}(z)$ toward a q -independent function for $\lambda \ll L$, which can be shown to be $\frac{1}{3}\lambda/L(z)$, and 2) the similarity of σ_z as a function of $\langle z \rangle$ for the three values of q at each λ (Figure 3b).

Discussion

We note that the transport equation used here neglects several well-known effects. Diffusion and drifts perpendicular to the field could reduce the intensity, especially for well-connected events, for which neighboring flux tubes have a lower intensity, but this should not significantly affect the propagation diagnostics discussed here. Adiabatic deceleration and convection were included in numerical simulations by Ruffolo (1995) and were shown to noticeably affect the propagation for ions of $\lesssim 20$ MeV/n and electrons of $\lesssim 10$ keV.

On the other hand, this approach does overcome the main limitation of the previous, analytic descriptions of coherent pulses (Earl 1976a, b), i.e., the assumption of a constant focusing length ($B \propto e^{-z/L}$). We find that several of their conclusions do not apply for the case of a realistic Archimedean spiral field. We find that for this case, the propagation speed is not constant, and does not exhibit distinct supercoherent and coherent régimes, but rather decreases steadily along with $\langle \mu \rangle_{eq}$. Other results from our simulations show that the pulse width increases roughly linearly with time, in contrast with the result for an exponential field that $\sigma_z \propto t^{1/2}$ (Earl 1974). Of course, these limitations do not diminish the importance of that seminal work.

It is hoped that these results will be applicable to studies of the time profile of particle injection from solar flares, or comparisons of the time of injection for different particle species. When a strong coherent pulse is observed, one can estimate λ from the anisotropy and the pulse width (Figure 3). A lack of consistency could indicate a finite injection width (if the pulse width is high), or shock acceleration outside the corona (if the anisotropy is high). One can derive the propagation time from λ , given an assumption or measurement for q . Subtracting the propagation time from the time of maximum then yields an estimated time of injection. Note that conditions with $\lambda \sim 1$

AU, corresponding to the highest mean free paths reported in the inner heliosphere, are sometimes called “scatter-free” conditions, with the implication that particles freely stream along the field at their maximum speed. However, our results show that even then, scattering significantly delays the arrival of the bulk of the pulse, while the “onset” is delayed somewhat less (see also Kallenrode and Wibberenz, 1990). In general, Figure 2 can be used to derive an accurate estimate of the propagation time.

Acknowledgments. The authors would like to thank the Laboratory for Astrophysics and Space Research at the University of Chicago for kindly allowing remote access to their computing facilities.

References

- Bieber, J. W., Numerical and analytic solutions of the Boltzmann equation for cosmic ray transport, Ph.D. thesis, 219 pp., Univ. of Maryland, July 1977.
- Earl, J. A., Coherent propagation of charged-particle bunches in random magnetic fields, *Astrophys. J.*, , 188, 379-397, 1974.
- Earl, J. A., The effect of adiabatic focusing upon charged-particle propagation in random magnetic fields, *Astrophys. J.*, , 205, 900-919, 1976a.
- Earl, J. A., Nondiffusive propagation of cosmic rays in the solar system and in extragalactic radio sources, *Astrophys. J.*, , 206, 301-311, 1976b.
- Earl, J. A., D. Ruffolo, H. L. Pauls, and J. W. Bieber, Comparison of three numerical treatments of charged particle transport, *Astrophys. J.*, , in press, 1995.
- Jokipii, J. R., Propagation of cosmic rays in the solar wind, *Rev. Geophys. Space Phys.*, 9, 27-87, 1971.
- Kallenrode, M.-B., G. Wibberenz, and S. Hucke, Propagation conditions of relativistic electrons in the inner heliosphere, *Astrophys. J.*, , 394, 351-356, 1992.
- Kallenrode, M.-B., and G. Wibberenz, Influence of Interplanetary Propagation on Particle Onsets, *Proc. 21st Internat. Cosmic Ray Conf. (Adelaide) 5*, 229, 1990.
- Ng, C. K., and K.-Y. Wong, Solar particle propagation under the influence of pitch-angle diffusion and collimation in the interplanetary magnetic field, *Proc. 16th Internat. Cosmic Ray Conf. (Kyoto) 5*, 252, 1979.
- Parker, E. N., Dynamics of the interplanetary gas and magnetic fields, *Astrophys. J.*, , 128, 664-676, 1958.
- Roelof, E. C., Propagation of solar cosmic rays in the interplanetary magnetic field, in *Lectures in High Energy Astrophysics*, edited by H. Ogelman and J. R. Wayland, pp. 111-135, Washington, DC, 1969.
- Ruffolo, D., Interplanetary transport of decay protons from solar flare neutrons, *Astrophys. J.*, , 382, 688-698, 1991.
- Ruffolo, D., Effect of adiabatic deceleration on the focused transport of solar cosmic rays, *Astrophys. J.*, , 442, 861-874, 1995 (astro-ph/9408056).

T. Khumlumlert and D. Ruffolo, Department of Physics, Faculty of Science, Chulalongkorn University, Bangkok 10330, Thailand.

April 6, 1995; revised June 2, 1995; accepted June 20, 1995.

Figure 1. Three stages in the evolution of a coherent pulse: the distribution function, F (vertical direction), vs. distance along the magnetic field, z , and pitch-angle cosine, μ , for $s = vt = 0.002, 0.01, \text{ and } 0.02$ AU, when $\lambda = 0.3$ AU, $q = 1.5$, and $F(t = 0)$ is concentrated at $z = 0$ and uniform in μ .

This preprint was prepared with AGU's L^AT_EX macros v4. File 9506133 formatted October 4, 2018.

Figure 2. Simulation results for the mean distance along the magnetic field, $\langle z \rangle$, vs. mean distance, $\langle z \rangle$, up to $s = 8.0$ AU for $q = 1.0$ (dotted lines), $q = 1.5$ (dashed lines), and $q = 1.9$ (solid lines). The dotted line corresponds to motion directly along the magnetic field.

Figure 3. a) Mean pitch-angle cosine, $\langle \mu \rangle = \langle v_z \rangle / v$, and b) pulse width, $\langle z \rangle$. For an explanation of the curves, see Figure 1. Solid circles show points for $\lambda = 1.0$ AU. That only curves for $\lambda = 1.0$ AU are extended to $s = 8.0$ AU.

Figure 4. a) Mean pitch-angle cosine, $\langle \mu \rangle$, vs. mean distance, $\langle z \rangle$, up to $s = 8.0$ AU for Figure 1, compared with $\langle \mu \rangle_{eq}$ for $\lambda = 0.3$ and $q = 1.0$ (○), 1.5 (⊕), and 1.9 (⊙) and λ and q as above.

Figure 5. a) Mean pitch-angle cosine, $\langle \mu \rangle$, vs. mean distance, $\langle z \rangle$, up to $s = 8.0$ AU for Figure 1, compared with $\langle \mu \rangle_{eq}$ (○) and highly focused (●) initial distributions, compared with $\langle \mu \rangle_{eq}$ (○).

Figure 2

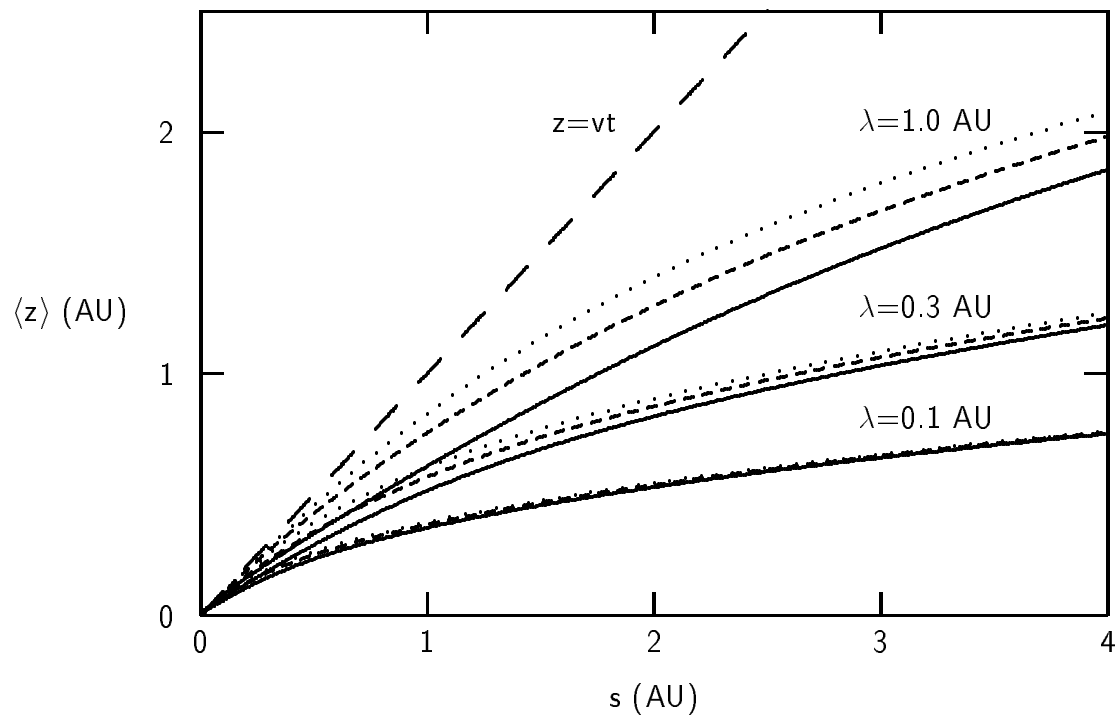


Figure 3

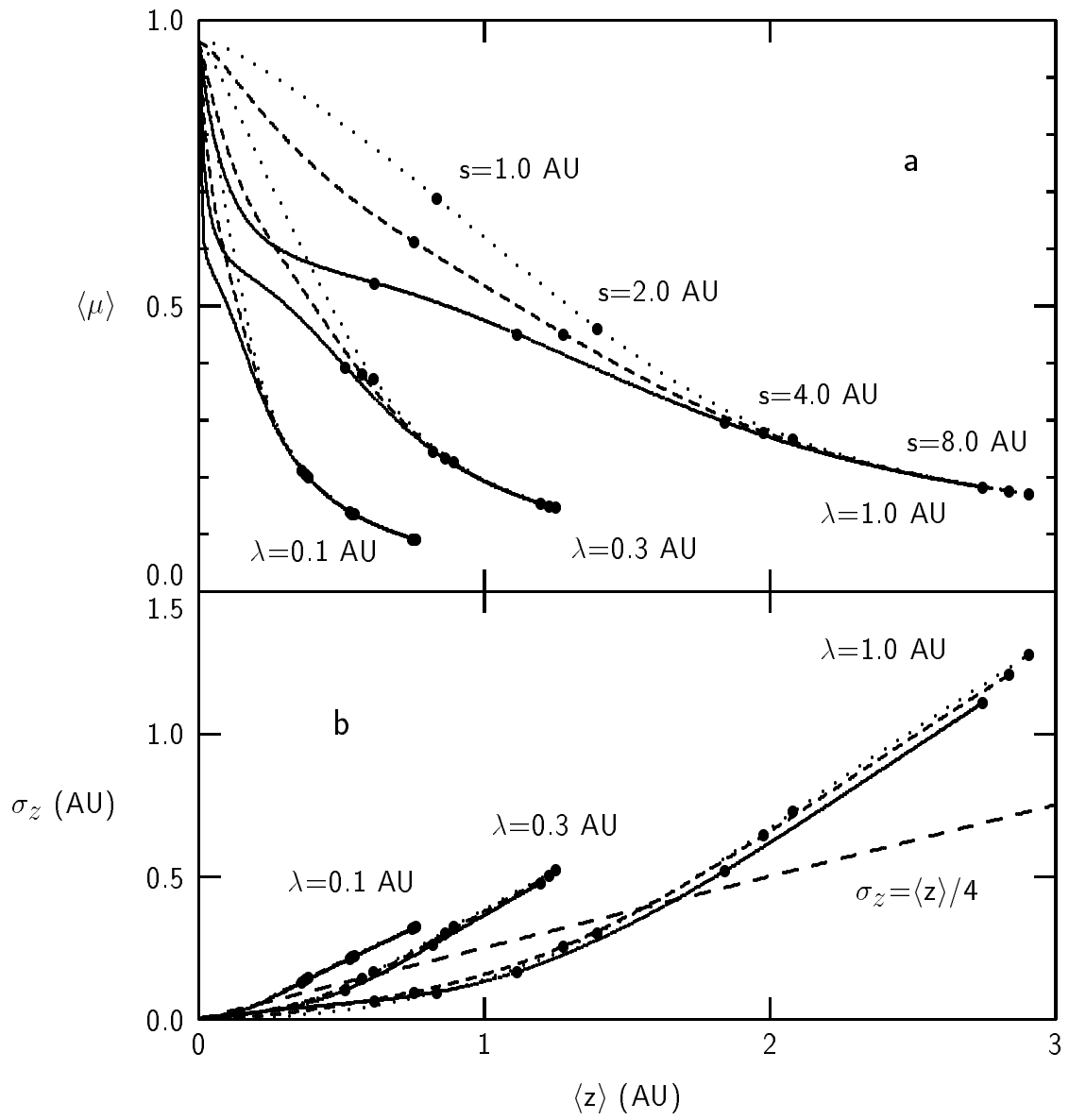


Figure 4

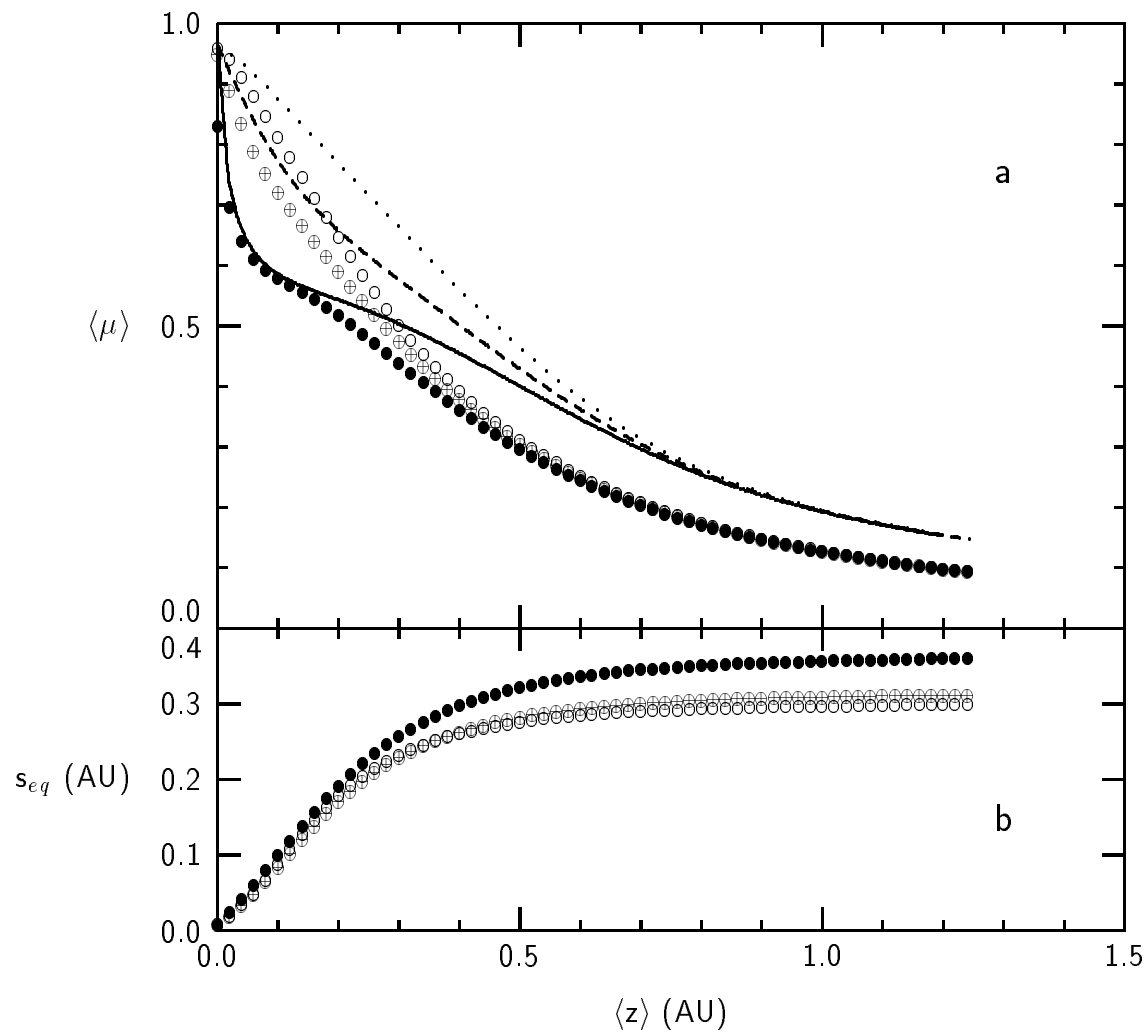


Figure 5

